Supporting Information

Rapid microwave-assisted synthesis of high-rate FeS_2 nanoparticles anchored on graphene for hybrid supercapacitors with ultrahigh energy density

Zhiqin Sun, Huiming Lin, Feng Zhang, Xue Yang, He Jiang, Qian Wang*, Fengyu Qu*

Key Laboratory of Photochemical Biomaterials and Energy Storage Materials, Heilongjiang Province, College of Chemistry and Chemical Engineering, Harbin Normal University, Harbin 150025, China

1. Experimental

1.1. Materials

Cobalt chloride hexahydrate ($CoCl_2 \cdot 6H_2O$, AR), urea ($CO(NH_2)_2$, AR), potassium hydroxide (KOH, AR), nickel nitrate hexahydrate ($Ni(NO_3)_2 \cdot 6H_2O$, AR), ferrous sulfate ($FeSO_4 \cdot 7H_2O$, AR), sodium thiosulfate pentahydrate ($Na_2S_2O_3 \cdot 5H_2O$, AR), sodium polyacrylate (PAAS), sulfuric acid (H_2SO_4, 98 wt.%), potassium permanganate ($KMnO_4$, AR), hydrogen peroxide (H_2O_2) were purchased from Sinopharm Chemical Reagent Co. Ltd. Sodium sulfide nonahydrate ($Na_2S \cdot 9H_2O$, 99.99 wt.%) was obtained from Aladdin (Shanghai).

1.2. Synthesis of FeS_2/GNS composite

Graphene oxide (GO) was prepared through modified Hummers method as reported before.[1] FeS_2/GNS composite was synthesized by using ultra-fast microwave-assisted hydrothermal method. In brief, 30 mL of the GO solution (0.16 mg mL^{-1}) was subject to ultrasonic vibration for 20 min. Then 0.25 mmol of $FeSO_4 \cdot 7H_2O$ and 0.5

*Corresponding authors.
E-mail addresses: wangqianhrb@163.com (Q.Wang); qufengyuhsd@163.com (F.Y.Qu).

mmol of $Na_2S_2O_3·5H_2O$ was added into the above solution and stirred for another 20 min. Subsequently, the as-prepared solution was transferred into a microwave reactor and heated at 180 °C with a power of 300 W for 5 min. Finally, the sample was centrifuged and washed using ultrapure water for several times and dried in an oven at 80 °C for 12 h. Pure FeS_2 was also synthesized without the use of GNS. For the control experiment, FeS_2/GNS-1 and FeS_2/GNS-2 composites had been also prepared by the similar hydrothermal route with 0.16 mmol of $FeSO_4·7H_2O$, 0.32 mmol of $Na_2S_2O_3·5H_2O$ and 0.42 mmol of $FeSO_4·7H_2O$, 0.84 mmol of $Na_2S_2O_3·5H_2O$, respectively.

1.3. Synthesis of $Ni(OH)_2$@Co_9S_8 composite

In a typical synthesis of $Co(CO_3)_{0.35}Cl_{0.20}(OH)_{1.10}$ precursor, $CoCl_2·6H_2O$ (2.5 mmol) and urea (2.5 mmol) were dissolved in 40 mL of deionized water under stirring and transferred into a 50 mL Teflon-lined stainless steel autoclave, which was maintained at 100 °C for 2 h. The pink precipitate was washed with deionized water and dried at 80 °C. Afterwards, 1 mmol of as-prepared precursor was dispersed in 40 mL of deionized water, and then, 3 mmol $Na_2S·9H_2O$ was added into the dispersion. After magnetic stirring for 1 h, the dispersion was transferred into a 50 mL Teflon–lined stainless steel autoclave at 160 °C for 12 h. Finally, the black product was centrifuged and washed by deionized water and the Co_9S_8 nanotube was synthesized.

$Ni(OH)_2$@Co_9S_8 composite was typically prepared as follows: the mixture contained 30 mL of Co_9S_8 nanotube dispersion (1 mg mL^{-1}) and 1 M $Ni(NO_3)_2$ was stirred for a few minutes, and then the pH of the whole dispersion was adjusted to 9 with ammonia (5 wt.%). Finally, the precipitate was washed and dried in a vacuum oven at 80 °C for 12 h. Pure $Ni(OH)_2$ was also prepared for comparison under the same

procedure without the addition of Co_9S_8 nanotube.

1.4. Characterization

X-ray diffraction (XRD) equipped with CuKα radiation (λ = 0.15406 nm) was used to characterize the crystallographic structures of all materials. Scanning electron microscope (SEM, Hitachi S–4800) and transmission electron microscope (TEM, Tecnai F20) were conducted to characterize the micromorphology. X-ray photoelectron spectroscopy (XPS, PHI 5000 ESCA) was carried out to investigate the valence state and composition of materials. Raman spectra of the products were characterized by Micro-Raman spectrometer (J-Y; HR800, France) under excitation wavelength of 488 nm. Thermogravimetric analysis (TGA) was used to calculate the content of graphene nanosheets in the composites. Nitrogen adsorption–desorption isotherms were measured at 77 K on a Quantachrome NOVA-3000 system.

1.5. Electrochemical measurements

The working electrodes were prepared as follows: First, the electroactive materials, carbon black and poly (tetrafluoroethylene) were mixed in a mass ratio of 75:20:5 and dispersed in ethanol. Then the resulting mixture was coated onto the nickel foam substrate (1×1 cm^2), which was followed by drying at 60 °C for 12 h in an oven. The as-prepared materials (mass loading: ~ 3 mg cm^{-2}) was used as working electrode with 2 M KOH solution as electrolyte. A three-electrode system was used to investigate the electrochemical performances of the individual electrodes. A platinum foil (1 cm^2) and Hg/HgO were used as the counter and the reference electrodes, respectively. Cyclic voltammetry (CV) and chronopotentiometry were performed on a CHI660E within -1.1 to 0 V and the electrochemical impedance (EIS) were carried out in the frequency range

from 100 kHz to 0.01 Hz at open circuit potential with an AC amplitude of 5 mV. The specific capacity of the anode and cathode could be calculated based on the galvanostatic charge/discharge curves by the following equation:

$$C_m = I\Delta t / m\Delta V \quad \text{(S1)}$$

where C_m, I, m, Δt and ΔV are the specific capacity, current, mass, discharge time and potential range of the active material.

1.6. Fabrication of hybrid supercapacitor device

PAAS-KOH gel electrolyte was prepared as follows: 2.5 g PAAS was dissolved in 30 mL of 2 M KOH aqueous solution and stirred until the solution became homogeneous and clear. FeS_2/GNS and $Ni(OH)_2@Co_9S_8$ electrodes, served as the anode and cathode, respectively, were coated with the gel electrolyte and separated with a piece of cellulose paper to fabricated all-solid-state hybrid supercapacitor. The mass balance of the anode and cathode should obey the relationships as follows:

$$q_+ = q_- \quad \text{(S2)}$$

$$q = CVm \quad \text{(S3)}$$

where q is the stored charge, C is the specific capacity, V is the potential range and the m is the mass of the active material.

Specific energy and power density of the hybrid supercapacitor device were calculated based on the following equations:

$$E = \int IV\mathrm{d}t \quad \text{(S4)}$$

$$P = \frac{E}{t} \quad \text{(S5)}$$

where E, I, V, t and m is the energy density, current, voltage, discharge time and mass of the active materials of two electrodes.

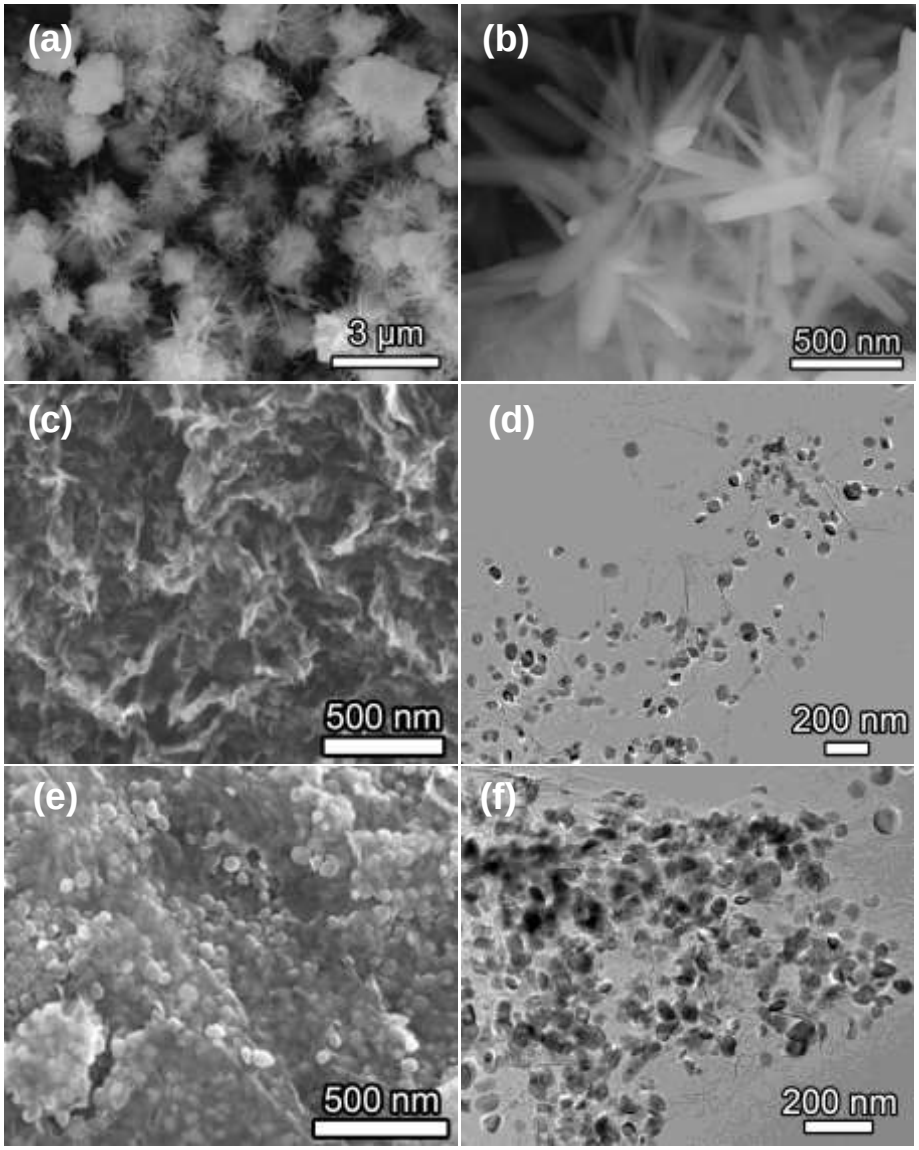

Fig. S1 (a, b) SEM images of pure FeS_2. (c) SEM and (d) TEM images of FeS_2/GNS-1, (e) SEM and (f) TEM images of FeS_2/GNS-2.

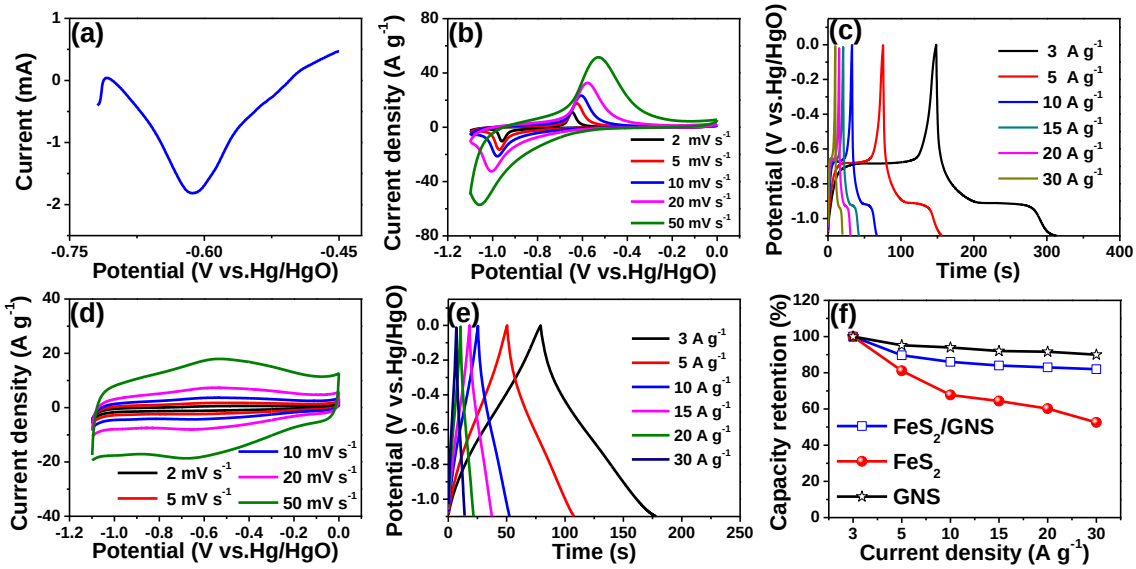

Fig. S2 (a) SWV curve of FeS_2/GNS electrode. (b) CV curves at different scan rates and (c) galvanostatic charge-discharge curves at various current densities of pure FeS_2 electrode. (d) CV curves at different scan rates and (e) galvanostatic charge-discharge curves at various current densities of GNS electrode. (f) Rate capability of pure FeS_2, GNS and FeS_2/GNS electrodes.

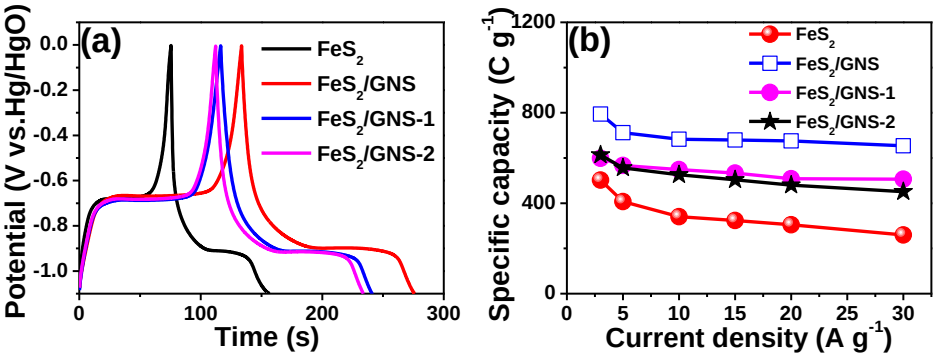

Fig. S3 (a) Galvanostatic charge/discharge curves of pure FeS_2, FeS_2/GNS, FeS_2/GNS-1 and FeS_2/GNS-2 electrodes at 5 A g^{-1} and (b) specific capacity of all the electrodes at various current densities.

Table S1 Integration of specific capacitance and rate capabilities of various electrodes reported previously based on Fe-based anode materials.

Electrode materials	Electrolyte	Potential range	Capacitance ($F\ g^{-1}$)	Capacitance retention	Ref.
Fe_3O_4/carbon nanosheets	6 M KOH	-1.1 to -0.2 V	586 (0.5 $A\ g^{-1}$)	58% (10 $A\ g^{-1}$)	2
3D Fe_3O_4/rGO	2 M KOH	-1.0 to 0.4 V	455 (8 $mV\ s^{-1}$)	70% (27 $mV\ s^{-1}$)	3
Fe_2O_3@Nickel nanotube	1 M Na_2SO_4	-0.8 to 0 V	418.7 (10 $mV\ s^{-1}$)	42% (200 $mV\ s^{-1}$)	4
FeOOH nanorods/graphene	1 M LiOH	-1.15 to 0.1 V	326 (0.5 $A\ g^{-1}$)	90% (10 $A\ g^{-1}$)	5
Fe_3O_4 particles/graphene	1 M KOH	-1 to 0.1 V	220.1 (0.5 $A\ g^{-1}$)	61% (5 $A\ g^{-1}$)	6
Fe_2O_3 particles/graphene	1 M KOH	-1.05 to -0.3 V	908 (2 $A\ g^{-1}$)	68.8% (50 $A\ g^{-1}$)	7
α-Fe_2O_3@MnO_2	3 M KOH	-0.4 to 0.5 V	289 (1 $A\ g^{-1}$)	40% (5 $A\ g^{-1}$)	8
FeS_2/GNS	**2 M KOH**	**-1.1 to 0 V**	**721 (3 $A\ g^{-1}$)**	**82% (30 $A\ g^{-1}$)**	**This work**

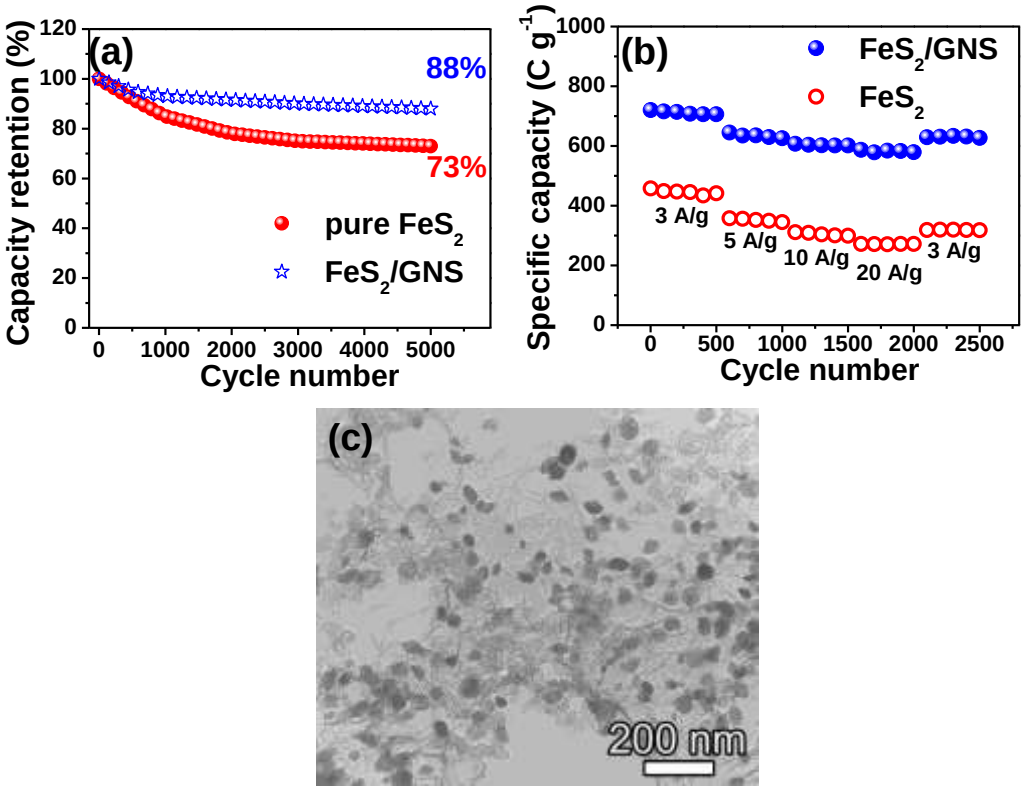

Fig. S4 (a) Cycling performance of pure FeS_2 and FeS_2/GNS electrodes measured at 20 A g^{-1} for 5000 cycles. (b) Cycling graph of pure FeS_2 and FeS_2/GNS electrodes at different current densities. (c) TEM image of FeS_2/GNS electrode after cycling test for 2500 cycles.

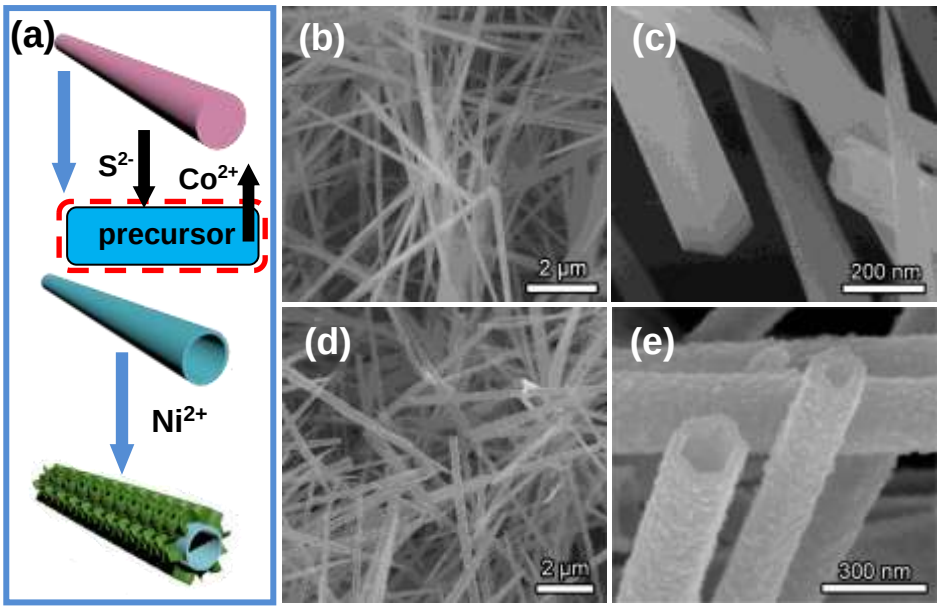

Fig. S5 (a) Schematic illustration of the synthesis process of hierarchical $Ni(OH)_2@Co_9S_8$ composite. SEM images of (b, c) precursor and (d, e) Co_9S_8.

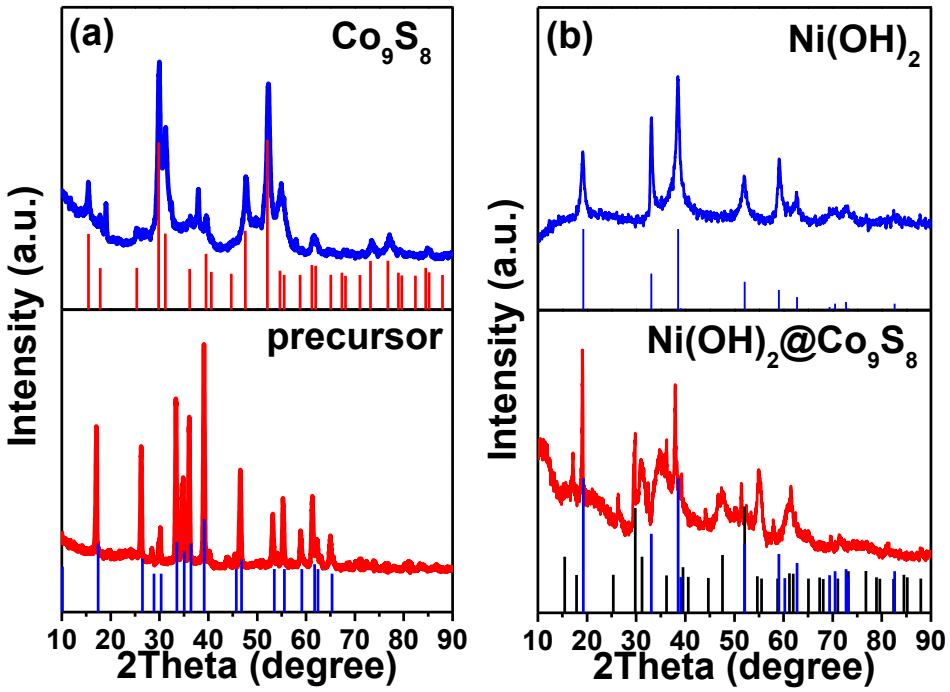

Fig. S6 XRD patterns of (a) Co_9S_8 and precursor, (b) $Ni(OH)_2$ and $Ni(OH)_2@Co_9S_8$ composite.

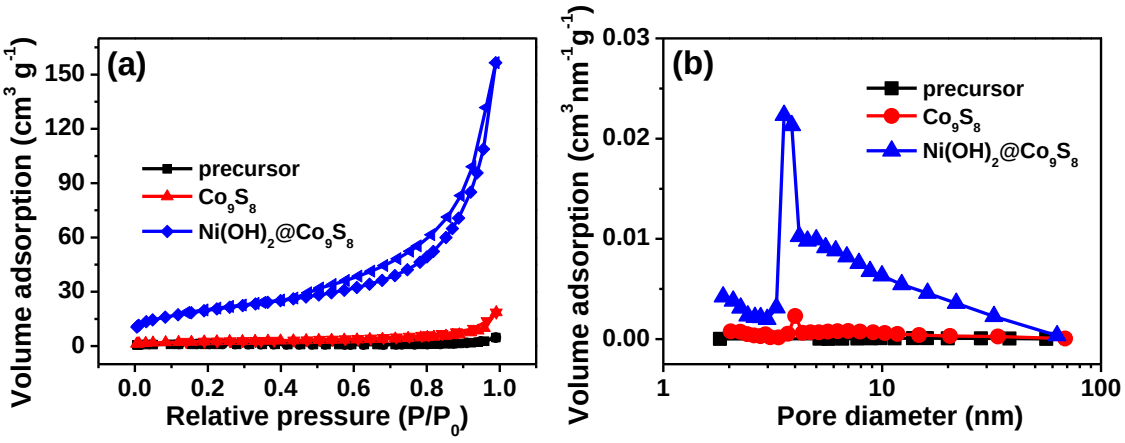

Fig. S7 (a) N_2 adsorption-desorption isotherms and (b) pore size distribution of the precursor, Co_9S_8 and $Ni(OH)_2@Co_9S_8$ composite.

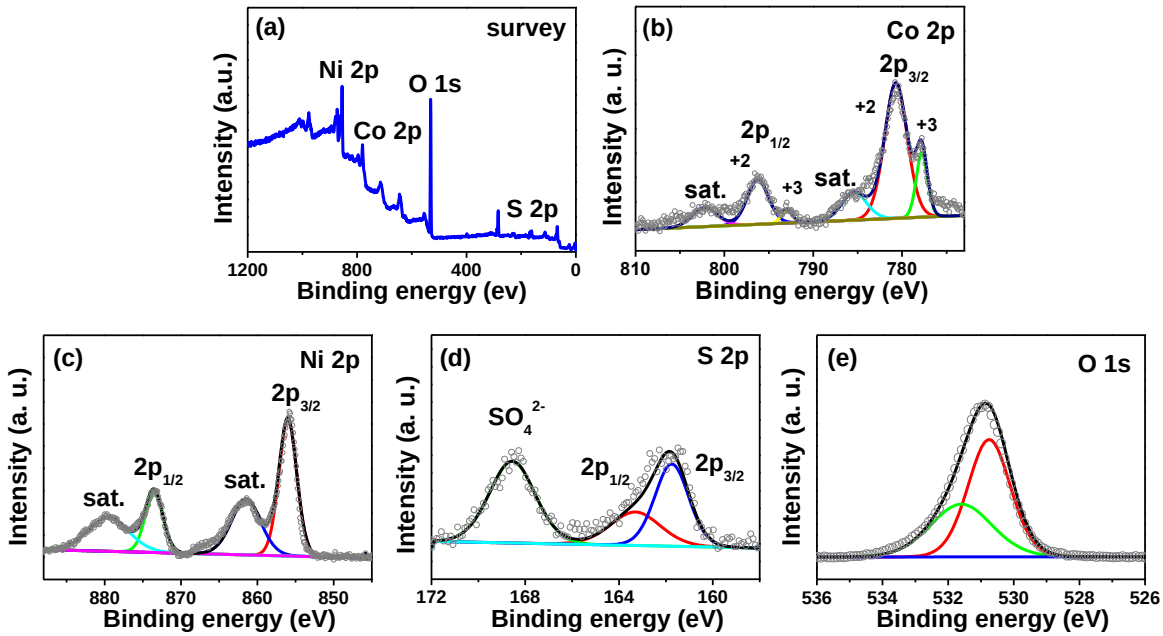

Fig. S8 XPS spectra of (a) survey, (b) Co 2p, (c) Ni 2p, (d) S 2p and (e) O 1s.

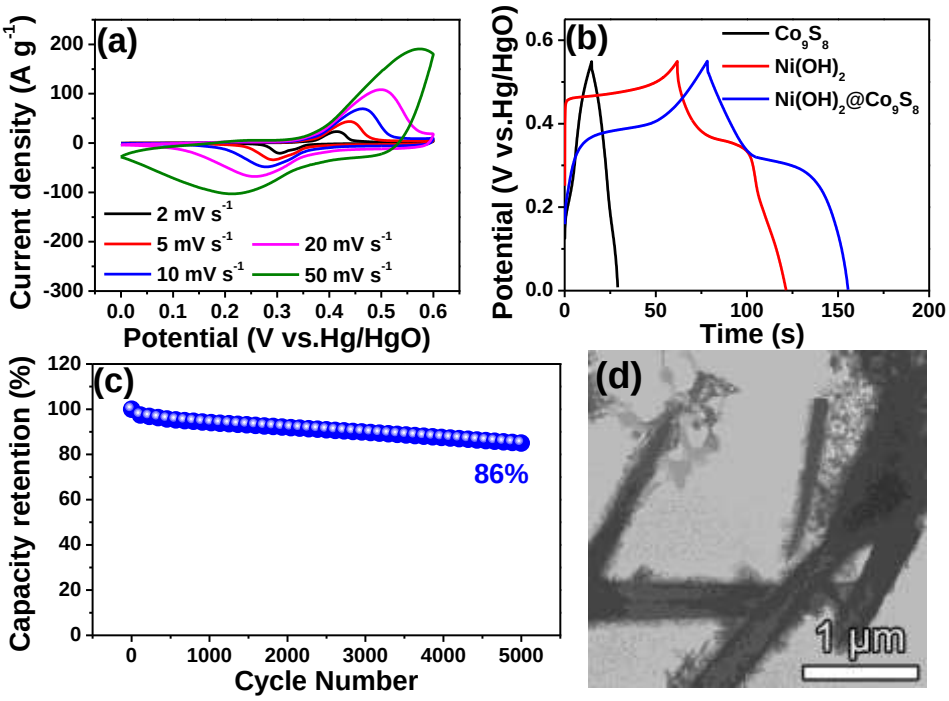

Fig. S9 (a) CV curves of $Ni(OH)_2@Co_9S_8$ electrode at various scan rates. (b) Galvanostatic charge-discharge curves of Co_9S_8, $Ni(OH)_2$ and $Ni(OH)_2@Co_9S_8$ electrodes at the same current density of 10 A g^{-1}. (c) Cycling performance of the $Ni(OH)_2@Co_9S_8$ electrode measured at 20 A g^{-1} for 5000 cycles. (d) TEM image of $Ni(OH)_2@Co_9S_8$ electrode after cycling test for 5000 cycles .

Table S2 Integration of electrochemical performance of various ASC and hybrid supercapacitor devices based on Fe-based anode materials reported recently.

Hybrid supercapcitor device	Electrolyte	Voltage (V)	Energy density (Wh kg^{-1})	Power density (kW kg^{-1})	Ref.
$CoMoO_4$@$NiMoO_4$·xH_2O//Fe_2O_3	KOH-PVA	1.6	41.8	0.7	[9]
MnO_2//Fe_2O_3	$LiClO_4$-PVA	2.0	41	2.1	[10]
MWCNTs/MnO_2//Fe_2O_3	$K_3[Fe(CN)_6]$-Na_2SO_4	2.0	54.39	0.667	[11]
FeOOH//Co-Ni double hydroxides	KOH-PVA	1.6	86.4	11.6	[12]
NiOOH/Ni_3S_2/3D graphene//Fe_3O_4/ graphene	KOH-PVA	1.6	82.5	0.93	[13]
Co-Fe_3O_4NS@NG// $CoMnO_3$NG	3 M KOH	1.8	89.1	0.901	[14]
MnO_2/CC// γ-FeOOH/CC	1 M Li_2SO_4	1.8	37.4	16	[15]
$NiMoO_4$//FeOOH	2 M KOH	1.7	104	1.27	[16]
GF-CNT@Fe_2O_3// GF-$CoMoO_4$	2 M KOH	1.6	74.7	1.4	[17]
$NiCo_2O_4$/NiO//Fe_2O_3	1 M KOH	1.6	19	0.157	[18]
SiC@$NiCo_2O_4$/$Ni(OH)_2$//SiC @Fe_2O_3	2 M KOH	1.8	45	26.1	[19]
NiO//α-Fe_2O_3	1 M KOH	1.25	12.4	0.951	[20]
FeS_2/GNS// $Ni(OH)_2$@Co_9S_8	**PAAS-KOH**	**1.7**	**95.8**	**0.949**	**This work**

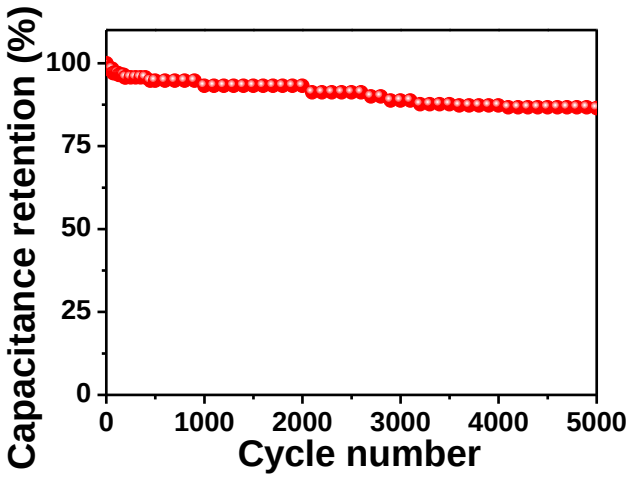

Fig. S10 Cycling performance of the hybrid supercapacitor device measured at 15 A g^{-1} for 5000 cycles.

Reference

1. J. Chen, Y. Li, L. Huang, C. Li and G. Shi, *Carbon*, 2015, **81**, 826-834.
2. H. Fan, R. Niu, J. Duan, W. Liu and W. Shen, *ACS Appl. Mater. Interfaces*, 2016, **8**, 19475-19483.
3. R. Kumar, R. K. Singh, A. R. Vaz, R. Savu and S. A. Moshkalev, *ACS Appl. Mater. Interfaces*, 2017, **9**, 8880-8890.
4. Y. Li, J. Xu, T. Feng, Q. Yao, J. Xie and H. Xia, *Adv. Funct. Mater.*, 2017, **27**, 1606728.
5. L.-F. Chen, Z.-Y. Yu, J.-J. Wang, Q.-X. Li, Z.-Q. Tan, Y.-W. Zhu and S.-H. Yu, *Nano Energy*, 2015, **11**, 119-128.
6. Q. Wang, L. Jiao, H. Du, Y. Wang and H. Yuan, *J. Power Sources*, 2014, **245**, 101-106.
7. H. Wang, Z. Xu, H. Yi, H. Wei, Z. Guo and X. Wang, *Nano Energy*, 2014, **7**, 86-96.
8. G. Nie, X. Lu, M. Chi, Y. Zhu, Z. Yang, N. Song and C. Wang, *Electrochim. Acta*, 2017, **231**, 36-43.
9. J. Wang, L. Zhang, X. Liu, X. Zhang, Y. Tian, X. Liu, J. Zhao and Y. Li, *Sci. Rep.*, 2017, **7**, 41088.
10. N. R. Chodankar, D. P. Dubal, G. S. Gund and C. D. Lokhande, *Energy Tech.*, 2015, **3**, 625-631.
11. N. R. Chodankar, D. P. Dubal, A. C. Lokhande, A. M. Patil, J. H. Kim and C. D. Lokhande, *Sci. Rep.*, 2016, **6**, 39205.
12. J. Chen, J. Xu, S. Zhou, N. Zhao and C.-P. Wong, *Nano Energy*, 2016, **21**, 145-153.
13. T. W. Lin, C. S. Dai and K. C. Hung, *Sci. Rep.*, 2014, **4**, 7274.
14. M. Guo, J. Balamurugan, X. Li, N. H. Kim and J. H. Lee, *Small*, 2017, **13**.
15. Y. C. Chen, Y. G. Lin, Y. K. Hsu, S. C. Yen, K. H. Chen and L. C. Chen, *Small*, 2014, **10**, 3803-3810.
16. K. A. Owusu, L. Qu, J. Li, Z. Wang, K. Zhao, C. Yang, K. M. Hercule, C. Lin, C. Shi, Q. Wei, L. Zhou and L. Mai, *Nat. Commun.*, 2017, **8**, 14264.
17. C. Guan, J. Liu, Y. Wang, L. Mao, Z. Fan, Z. Shen, H. Zhang and J. Wang, *ACS Nano*, 2015, 5198-5207.
18. A. Shanmugavani and R. K. Selvan, *Electrochim. Acta*, 2016, **189**, 283-294.
19. J. Zhao, Z. Li, X. Yuan, Z. Yang, M. Zhang, A. Meng and Q. Li, *Adv. Energy Mater.*, 2018, 1702787.
20. S. Zhang, B. Yin, Z. Wang and F. Peter, *Chem. Eng. J.*, 2016, **306**, 193-203.